Acta Crystallographica Section D
Biological Crystallography
ISSN 0907-4449

Structure of acutolysin-C, a haemorrhagic toxin from the venom of *Agkistrodon acutus*, providing further evidence for the mechanism of the pH-dependent proteolytic reaction of zinc metalloproteinases

Xue-yong Zhu,[a] Mai-kun Teng[a] and Li-wen Niu[a,b]*

[a]Department of Molecular and Cell Biology and Laboratory of Structural Biology, School of Life Sciences, University of Science and Technology of China, 96 Jinzhai Road, Hefei, Anhui, 230026, People's Republic of China, and [b]National Laboratory of Biomacromolecules, Institute of Biophysics, CAS, 15 Datun Road, Beijing, 100101, People's Republic of China

Correspondence e-mail: mkteng@ustc.edu.cn

Received 8 March 1999
Accepted 27 July 1999

PDB Reference: acutolysin-C, 1qua.

The structure of acutolysin-C, a haemorrhagic zinc metalloproteinase from the venom of *Agkistrodon acutus*, has been analyzed and refined at 2.2 Å resolution. The space group of the crystal is $P2_12_12_1$, with unit-cell dimensions a = 46.84, b = 49.52, c = 95.34 Å. One molecule was found in each asymmetric unit. The phasing problem was solved by the molecular-replacement program *AMoRe*. Crystallographic refinement was performed using *X-PLOR*, leading to final R and free R factors of 0.176 and 0.272, respectively. The residue sequence of acutolysin-C was determined mainly by electron density. No density was found for the first residue at the N-terminus and the last two residues at the C-terminus, which was also the case for most other P-I class snake-venom metalloproteinases (SVMPs). Acutolysin-C has two highly conserved characteristic sequences His142-Glu143-*X*-*X*-His146-*X*-*X*-Gly149-*X*-*X*-His152 and Cys162-Ile163-Met164. The enzyme has three disulfide bridges: Cys117–Cys195, Cys157–Cys179 and Cys159–Cys162. The entire structure shows good agreement with that of other reported P-I class SVMPs and has two subdomains with a cleft in which one catalytic zinc ion is localized. However, the local conformation (especially the disulfide configurations), the coordination of the catalytic water molecules and some residue side chains differ compared with other P-I class SVMPs. The proteolytic activities of SVMPs are sensitive to the pH value. The molecular superpositions around the proteolytic active sites of all the P-I class SVMP crystal structures show that the distances between the zinc ion and its ligands are not correlated with the crystallization pH values, although the contact distances between the catalytic water molecule and the O atoms of the Glu143 carboxylate group in the neutral and weakly alkaline structures are shorter than those in weakly acidic structures, and the closer the crystallization pH value of one enzyme is to its optimal activity pH value, the shorter the contact distances. Overall, all P-I class SVMPs have similar conformations in the active-site cleft. The size of the active site is not correlated with the crystallization pH values or the proteolytic activities. The disulfide bridge Cys117–Cys195 is conserved in all crystal structures of P-I class SVMPs, whereas the conformation and number of disulfide bridges in the C-terminal subdomain differ. Acutolysin-C has no structural calcium ion, which may not affect the proteolytic activity or haemorrhagic activity directly.

1. Introduction

The snake-venom metalloproteinases (SVMPs, also known as adamalysins), together with the astacins, the matrix metallo-

proteinases (also known as matrixins or collagenases) and the serralysins (large bacterial proteases from *Serratia*, *Erwinia* and *Pseudomonas*), form a family of proteolytic enzymes for which the designation 'metzincins' has been proposed, as all four kinds of proteinases exhibit the characteristic consensus motif HE*xx*H*xx*G*xx*H, with the three histidine residues being involved in binding the catalytically essential zinc ion, and share a conserved methionine residue beneath the active-site metal as part of a superimposable 'Met-turn' (Bode *et al.*, 1994; Gomis-Rüth *et al.*, 1993, 1994; Hooper, 1994; Stöcker *et al.*, 1995). A large number of SVMPs with different molecular weights and biological functions have been isolated from the crotalid and viperous venoms; some of these are also named haemorrhagins or haemorrhagic toxins owing to their capability to destroy the structures of the basement membrane and the extracellular matrix surrounding capillaries and small vessels and cause local haemorrhage after injection into experimental animals (Ownby, 1990; Bjarnason & Fox, 1994), whilst others are non-haemorrhagic. The SVMPs can be classified into four classes, P-I, P-II, P-III and P-IV, according to the number and organization of the domains contained. The largest SVMPs (P-IV class) contain a proteinase domain, a disintegrin-like domain, a cysteine-rich domain and a lectin domain sequentially from the N-terminus to the C-terminus. The smallest SVMPs (P-I class) contain only a proteinase domain. The proteinase domain is represented by three forms: a two-disulfide, a three-disulfide and a four-disulfide structure (Chung *et al.*, 1996). The P-I class can be further divided into two subclasses: P-IA, having strong haemorrhagic activities, and P-IB, having weaker or no haemorrhagic activities (Bjarnason & Fox, 1995). Additionally, a variety of organisms including mammals, reptiles and invertebrates have been found to produce a family of multi-domain proteins generally termed ADAMs, which are proteins containing a disintegrin-like and metalloproteinase domain (Wolfsberg *et al.*, 1995). In addition to the domain structure described for the P-III class of SVMPs, the ADAMs have an epidermal growth-factor-like domain, a transmembrane domain and a cytoplasmic domain (Jia *et al.*, 1996) and are also considered to be members of the reprolysin family (Bjarnason & Fox, 1995).

In the SVMP family, crystal structures of three P-IB subclass SVMPs with or without inhibitor have been determined: adamalysin II from *Crotalus adamanteus* venom (Gomis-Rüth *et al.*, 1994, 1998; Cirilli *et al.*, 1997), atrolysin C from *C. atrox* venom (Zhang *et al.*, 1994; Botos *et al.*, 1996) and H_2-proteinase from *T. flavoviridis* (Kumasaka *et al.*, 1996); the crystal structure of acutolysin-A, a member of the P-IA subclass SVMPs from *Agkistrodon acutus*, has also been determined (Gong *et al.*, 1998). Adamalysin II and atrolysin C are two-disulfide enzymes, whilst H_2-proteinase and acutolysin-A are three-disulfide enzymes. However, adamalysin II and H_2-proteinase are both non-haemorrhagic; in contrast, atrolysin C and acutolysin-A possess weak and strong haemorrhagic activities, respectively. These proteases are similar in terms of crystal structure. The proteolytic mechanism and the geometric characteristics of SVMPs binding to inhibitors have been analyzed (Gomis-Rüth *et al.*, 1994, 1998; Zhang *et al.*, 1994; Cirilli *et al.*, 1997); however, the detailed mechanisms of the proteolytic activity such as why the proteolytic activity is sensitive to pH value remain to be understood. As has been reported, most of the SVMPs show optimal activities under neutral or weakly alkaline conditions (Kurecki *et al.*, 1978; Bjarnason & Fox, 1987; Kumasaka *et al.*, 1996; Zhu, Zhu *et al.*, 1997).

The venom of Chinese mainland *A. acutus* contains plenty of potent haemorrhagins. Four haemorrhagins, acutolysin-A, acutolysin-B, acutolysin-C and acutolysin-D, have been purified and characterized (Xu *et al.*, 1981; Zhu, Gong *et al.*, 1997; Zhu, Zhu *et al.*, 1997). In contrast to other SVMPs whose crystal structures have been determined, acutolysin-C is an alkaline zinc metalloproteinase (pI > 9.0) and possesses weak haemorrhagic activity (Xu *et al.*, 1981). The crystallization and preliminary X-ray crystallographic analysis of acutolysin-C (Gong *et al.*, 1996, 1997) have been reported previously, but the amino-acid residue sequence, the number of intra-chain disulfide bridges and the metal ions which may occur in the protein are still unknown. The purpose of this paper is to provide details of the crystal structure and the possible 'crystallographic sequence' of acutolysin-C at 2.2 Å resolution and to discuss the mechanism by which the proteolytic activities of zinc metalloproteinases vary with the pH value.

2. Materials and methods

2.1. Crystallization and data collection

Acutolysin-C was purified as described previously (Gong *et al.*, 1996), with two chromatographic steps (DEAE-Sepharose Fast Flow and Sephacryl S-200). Crystals of acutolysin-C were grown at room temperature by the hanging-drop vapour-diffusion technique from protein solution [20 mg ml^{-1} buffered with Tris–HCl pH 7.5 containing 10%(*w*/*v*) PEG 4000] equilibrated against the precipitating solution [buffered with Tris–HCl pH 7.5 containing 20%(*w*/*v*) PEG 4000] for a week or longer.

Diffraction data were collected on a MAR Research imaging-plate system mounted on a X-ray generator (40 kV, 50 mA) with a sealed copper-target tube and a graphite monochromator at our laboratory. The crystal-to-detector distance was set to 150 mm. A total of 90 frames were recorded from one crystal at room temperature, with an oscillation angle range of 1.0° per frame. The data were integrated and scaled (Table 1) with *DENZO* and *SCALEPACK* (Otwinowski, 1993; Minor, 1993).

2.2. Structural determination and refinement

Acutolysin-C was located using the H_2-proteinase (Kumasaka *et al.*, 1996) as a model in rotation and translation searches with *AMoRe* (Navaza, 1994) from the *CCP*4 package (Collaborative Computational Project, Number 4, 1994). The metal ion, water molecules and the side chains of 61 highly variable residues of H_2-proteinase were excluded from the search model; the temperature factors of all remaining atoms were set to 20.0 Å^2. The clear rotation and translation solution

Table 1
Data collection and structural refinement of acutolysin-C structures.

Crystallization pH	7.5
Space group	$P2_12_12_1$
Unit-cell dimensions	
a (Å)	46.84
b (Å)	49.52
c (Å)	95.34
Number of molecules in asymmetric unit	1
Resolution range (Å)	8.0–2.2
Independent reflections	10704
Completeness (%)	90.7
Last-shell completeness (%)†	95.5
$R_{\rm merge}$‡	0.080
Last-shell $R_{\rm merge}$‡	0.263
Number of waters	105
Number of metal ions	1
$R_{\rm cryst}$ §	0.176
$R_{\rm free}$ §	0.272
Bond-length r.m.s. deviation (Å)	0.015
Bond-angle r.m.s. deviation (°)	1.85
Average temperature factors (Å^2)	
All atoms	22.84
Protein atoms	21.75
Main-chain atoms	20.89
Side-chain atoms	22.46
Water molecules	38.47

† The last shell is from 2.25–2.20 Å. ‡ $R_{\rm merge} = \sum|I - \langle I\rangle|/\sum\langle I\rangle$, where I is the observed diffraction intensity and $\langle I\rangle$ is the average diffraction intensity of several measurements of one reflection. The summation is over all reflections. § $R = \sum||F_o| - |F_c||/\sum|F_o|$, where F_o and F_c are the observed and calculated structure factors, respectively. The conventional crystallographic R factor ($R_{\rm cryst}$) and free R factors ($R_{\rm free}$) are calculated using the work and test reflection sets, respectively.

had a correlation coefficient of 66.2% and an R factor ($R_{\rm cryst}$) of 0.379 for all data in the resolution range 20.0–4.5 Å.

Expanding and using the data with $F_{\rm obs} > 2.0\sigma(F_{\rm obs})$ to 2.2 Å resolution, preliminary refinement of the model given by molecular replacement was performed using the simulated-annealing (SA) protocol of *X-PLOR* (Brünger, 1992*a*). A test data set containing 10% of the reflections was selected and reserved for the calculation and examination of the free R factor ($R_{\rm free}$; Brünger, 1992*b*) throughout the entire refinement process. Based on the electron-density maps ($2F_o - F_c$ map and $F_o - F_c$ map), the structure was rebuilt using the graphics programs *O* (Jones *et al.*, 1991) and *CHAIN* (Sack, 1988). The initial $R_{\rm cryst}$ and $R_{\rm free}$ were 0.424 and 0.437, respectively, and the initial $2F_o - F_c$ map generated by *X-PLOR* (Brünger, 1992*a*) showed that the model fitted the electron density well except for the main chains and side chains of residues 154–163 and 169–173 and the side chains of some other residues. 45 'bad' side chains which did not fit the electron density well were deleted; the main chains of residues 154–163 and 169–173 were retained, but their occupancy factors were set to zero in order to remove their contributions to the structural factors. $R_{\rm cryst}$ and $R_{\rm free}$ fell to 0.266 and 0.375, respectively, after several cycles of *X-PLOR* SA minimization in which the weighting scheme for diffraction term was skilfully adjusted as demonstrated by the falling $R_{\rm cryst}$ and $R_{\rm free}$.

At this point, the $2F_o - F_c$ map showed that a relatively strong peak of electron density representing the intrinsic Zn^{2+} ion was very clear at a position similar to that in other adamalysins (Gomis-Rüth *et al.*, 1994; Zhang *et al.*, 1994; Kumasaka *et al.*, 1996; Gong *et al.*, 1998). The main chains of all residues and the side chains of most residues could be identified unambiguously by their electron density. In order to find the differences between some side chains, *e.g.* Asp and Asn, Glu and Gln, Thr and Val, Lys and Met or His and Phe, the local environment around the residues, especially the ability to form hydrogen bonds and/or salt bridges with neighbouring groups, was taken into account, together with the alignment of the sequence homology of 24 SVMPs. After rebuilding the structures of all side chains and the main chains of residues 154–163 and 169–173, several cycles of restrained positional and individual temperature-factor refinements were performed alternately, which decreased $R_{\rm cryst}$ and $R_{\rm free}$ to 0.217 and 0.294, respectively. Three shells of water molecules were then added using the *X-PLOR* 3.851 program *WATERPICK* and refined using the restrained positional and individual temperature-factor refinements. The water molecules were located as peaks possessing electron density greater than 1.3σ in $2F_o - F_c$ maps and reasonable stereochemical geometry; the corresponding peaks in $F_o - F_c$ maps could also be found. The changes in $R_{\rm free}$ were monitored and only structures possessing decreased $R_{\rm free}$ were accepted and retained in the course of the entire model refinement mentioned above.

3. Results and discussion

3.1. Quality of the model

One zinc ion, 1497 non-H atoms and 105 water molecules were located and refined, leading to excellent stereochemical geometry and final $R_{\rm cryst}$ and $R_{\rm free}$ values of 0.176 and 0.272,

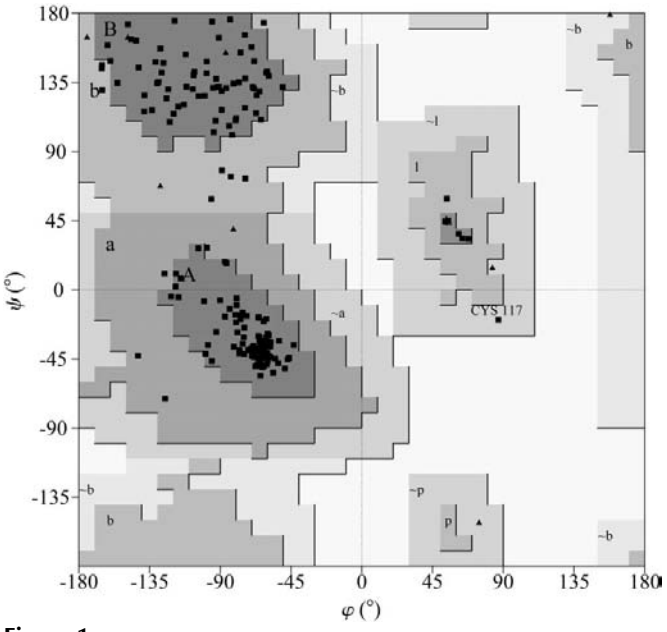

Figure 1
Ramachandran plot of acutolysin-C. The main-chain conformational angles (φ and ψ) of all non-glycine residues (indicated by a box), except for Cys117, lie within the allowed low-energy regions (indicated by solid boundaries). Glycine residues are indicated with a triangle. The plot was produced using *PROCHECK* (Laskowski *et al.*, 1993).

Table 2
Geometry of zinc ion binding environment, the number of disulfides and the haemorrhagic activity of acutolysin-C and other SVMPs for which crystal structures have been reported.

Data for adamalysin II derived from Gomis-Rüth *et al.* (1994) and Kurecki *et al.* (1978); data for atrolysin C derived from Zhang *et al.* (1994), Bjarnason & Fox (1987) and Bjarnason & Tu (1978); data for acutolysin-A derived from Gong *et al.* (1998), Zhu, Zhu *et al.* (1997) and Xu *et al.* (1981); data for H_2-proteinase derived from Kumasaka *et al.* (1996).

	Adamalysin II	Acutolysin-A	Atrolysin C (chain A)	Acutolysin-A	Acutolysin-C	H_2-proteinase
Crystallization pH value	5.0	5.0	6.8	7.5	7.5	8.0
Optimal pH for proteolytic activity	10.0	~8.8	8.3	~8.8	~7.0	~8.0
His142 $N^{\epsilon 2}$—Zn (Å)	2.09	2.05	2.01	2.07	2.05	2.39
His146 $N^{\epsilon 2}$—Zn (Å)	2.14	2.26	2.02	2.10	2.08	2.26
His152 $N^{\epsilon 2}$—Zn (Å)	2.11	2.27	2.02	2.09	1.88	2.19
Water—Zn (Å)	2.35	2.16	2.11	2.06	1.98	2.44
Water···Glu143 $O^{\epsilon 1}$ (Å)	4.11	4.19	4.15	3.84	3.95	3.42
Water···Glu143 $O^{\epsilon 2}$ (Å)	4.66	3.85	4.08	3.53	3.51	3.27
Number of disulfides	2	—	2	3	3	3
Minimum haemorrhagic dose (µg)	None	—	11.0	0.4	10.0	None

respectively, for the diffraction data to 2.2 Å resolution (Table 1). No residues were found in the disallowed regions of the Ramachandran plot (Fig. 1) and 92.3% of residues were in the most favoured regions. The residue Cys117 had conformational angles in the generously allowed regions, as observed in other reported adamalysins, which may be the result of the formation of the Cys117–Cys195 disulfide bond. The mean deviation of coordinates in the final model was estimated from a Luzzati plot (Luzzati, 1952) to be in the range 0.25–0.30 Å (data not shown). All residues except for the main chains of Ala155, Gly156, Ser169 and Ser170 fitted the electron density well in the refined structure (Fig. 2). The temperature factors for all groups, including the water molecules and zinc ion, were crystallographically acceptable (Table 1, Fig. 3).

The amino-acid residue sequence was determined mainly from the electron density (Table 2). No density was found for the first residue at the N-terminus and the last two residues at the C-terminus, which was also the case in most other P-I class SVMPs; it remains unknown whether these residues are absent or are crystallographically disordered. The recognition of several residues on the molecular surface (such as Ala35, Val50, Ala62, Ala155, Gly156, Ser158, Thr161, Lys181 and Ile190) was ambiguous owing to the unclear electron density; however, the highly conserved residues at the zinc ion binding site and putative calcium ion binding site fitted the electron density well.

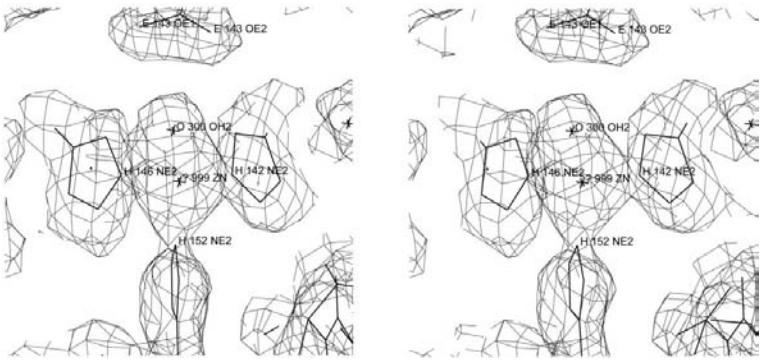

Figure 2
The active-site structure of acutolysin-C superimposed with the electron densities. The plot was produced using *CHAIN* (Sack, 1988).

3.2. Crystallographic sequence and overall structure

The current 'crystallographic sequence' of acutolysin-C has a high homology with other zinc metalloproteinases of low molecular weight (Fig. 4). Acutolysin-C has three disulfide bridges (Cys117–Cys195, Cys157–Cys179 and Cys159–Cys162). Acutolysin-C also has two highly conserved characteristic sequences His142-Glu143-*X*-*X*-His146-*X*-*X*-Gly149-*X*-*X*-His152 and Cys162-Ile163-Met164. Both acutolysin-C and acutolysin-A are purified from the same venom; acutolysin-A is a acidic protein, whilst acutolysin-C is alkaline. Based on the current 'crystallographic sequence', the sequence alignment between acutolysin-C and acutolysin-A shows about 50% homology; clearly, the accurate percentage homology needs to be further confirmed after determining the correct sequence of acutolysin-C. Also, the entire amino-acid sequence of acutolysin-C should be determined by chemical and/or cDNA sequencing to diminish the ambiguity in the recognition of residues owing to the relatively poor diffraction resolution limit of the crystals.

The general folding of the polypeptide chain in acutolysin-C is essentially similar to that in other P-I class SVMPs (Gomis-Rüth *et al.*, 1994; Zhang *et al.*, 1994; Kumasaka *et al.*, 1996; Gong *et al.*, 1998). Its secondary structure is composed of two structural domains separated by a cleft (Fig. 5). The 'upper' domain (residues 2–152) consists of a central highly twisted five-stranded β-sheet with α-helices arranged on the both sides of this central sheet. The central β-sheet has four parallel β-strands: strand I (residues 6–14), strand II (residues 49–58), strand III (residues 94–99) and strand V (residues 123–127). Strand IV (residues 108–112), which faces the cleft, is antiparallel. Strands I and II are connected through a

short helix *A* (residues 16–21) and a long helix *B* (residues 26–45); helix *C* (residues 71–86), which covers large parts of the three central β-strands (β-strands I, II and III) together with two loop segments, is on the opposite side to helix *A*, helix *B* and helix *D* (residues 133–147). The 'lower' domain (residues 153–198) consists of a long α-helix (helix E, residue 178–191) and a complicated loop region, which contains the Met-turn and is stabilized by two disulfide bridges. The bottom of the cleft is occupied by a catalytic active centre consisting of the Zn atom and its chelators.

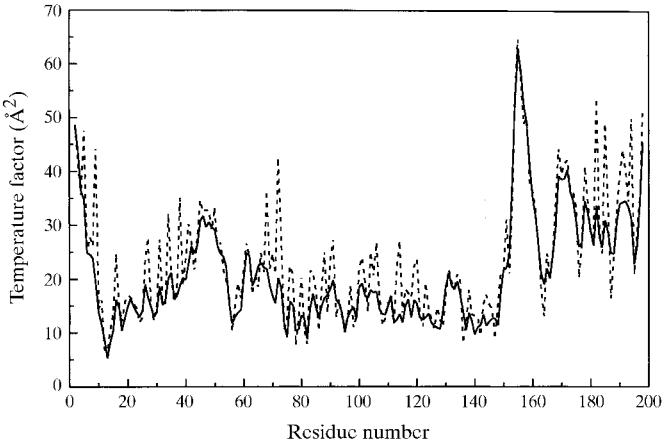

Figure 3
The temperature-factor distribution of main chains (solid line) and side chains (dashed line) of acutolysin-C.

	1	10	20	30	40	50
Acutolysin-C	-PAPQTSIELFLIVDHSMYAKYNSNSSKITTTLKARVNIMNAIYSSLNLV					
Acutolysin-A	STEFQRYMEIVIVVDHSMVKKYNGDSNSIKAWVYEMINTITESYSYLNID					
Adamalysin II	<EQNLPQRYIELVVVADRRVFMKYNSDLNIIRTRVHEIVNIINEFYRSLNIR					
Atrolysin C	<EQNLPQRYIELVVVADHRVFMKYNSDLNTIRTRVHEIVNFINGFYRSLNIH					
H_2-proteinase	ERFPQRYIELAIVVDHGMYKKYNQNSDKIKVRVHNMVNHINEMYRPLNIA					

	51	60	70	80	90	100
Acutolysin-C	ITLSGIEMWSAADLITVQSSSRNTLKLFASWRETDLLKRTSNDNAQLLTA					
Acutolysin-A	IILSGLEIWSEKDLINVEASAANTLKSFGEWRAKDLLHRISHDNAQLLTA					
Adamalysin II	VSLTDLEIWSGQDFITIQSSSSNTLNSFGEWRERVLLTRKRHDNAQLLTA					
Atrolysin C	VSLTDLEIWSNEDQINIQSASSDTLNAFAEWRETDLLNRKRHDNAQLLTA					
H_2-proteinase	ISLNRLNIWSKKDLITVKSASNVTLESFGNWRETVLLKQQNNDCAHLLTA					

	101	110	120	130	140	150
Acutolysin-C	TNFNGNTVGLAYLKTMCNSKYSVGLIQDHSAIPLLMAVTMAHELGHNLGM					
Acutolysin-A	TDFDGATIGLAYTASMCNPKRSVGIIQDHSSVNRLVAITLAHEMAHNLGV					
Adamalysin II	INFEGKIIGKAYTSSMCNPRSSVGIVKDHSPINLLVAVTMAHELGHNLGM					
Atrolysin C	IELDEETLGLAPLGTMCDPKLSIGIVQDHSPINLLMGVTMAHELGHNLGM					
H_2-proteinase	TNLNDNTIGLAYKKGMCNPKLSVGLVQDYSPNVFMVAVTMTHELGHNLGM					

	151	160	170	180	190	198
Acutolysin-C	NHDGAG.CSC..ATCIMAPVLSSGPAKSFSDCSKHDYQSFLTIHKPQCLLN					
Acutolysin-A	SHDEGS.CSCGGKSCIMSPSISDETSKYFSDCSYIQCRDYIAKENPPCILN					
Adamalysin II	EHDGKD.CLRGASLCIMRPGLTPGRSYEFSDDSMGYYQKFLNQYKPQCILNKP					
Atrolysin C	EHDGKD.CLRGASLCIMRPGLTKGRSYEFSDDSMHYYERFLKQYKPQCILNKP					
H_2-proteinase	EHDDKDKCKCEA..CIMSDVISDKPSKLFSDCSKNDYQTFLTKYNPQCILNA					

Figure 4
Alignment of the current sequence of acutolysin-C from *A. acutus* with some snake-venom metalloproteinases. <E denotes 5-pyrrolidone-2-carboxylic acid. Acutolysin-A is a strongly haemorrhagic proteinase from Chinese mainland *A. acutus* (Gong *et al.*, 1998). Adamalysin II is a non-haemorrhagic proteinase from the Eastern diamondback rattlesnake *C. adamanteus* (Gomis-Rüth *et al.*, 1994). Atrolysin C is a weakly haemorrhagic proteinase from the Western diamondback rattlesnake *C. atrox* (Shannon *et al.*, 1989) H_2-proteinase is a non-haemorrhagic proteinase from *T. flavoviridis* (Takeya *et al.*, 1989).

3.3. The pH-dependent proteolytic activity

The zinc ion binding site of acutolysin-C is similar to that of other P-I class SVMPs (Fig. 2). The zinc ion is located at the bottom of the active-site cleft and is ligated by three $N^{\varepsilon 2}$ atoms of His142, His146 and His152 and the O atom of a putative catalytic solvent molecule Water300; the water molecule is close to the O atoms of the Glu143 carboxylate group.

After determination of the astacin and adamalysin II structures (Bode *et al.*, 1992; Gomis-Rüth *et al.*, 1994), it was proposed that Glu143 could polarize the zinc ion coordinated water molecule Water300, prompting its nucleophilic attack on the scissile peptide bond of a polypeptide chain substrate. The key role of this water molecule was confirmed by the structures of the complexes of atrolysin C with inhibitors (Zhang *et al.*, 1994). It was also indicated that the carbonyl group of the scissile peptide bond will point towards the zinc

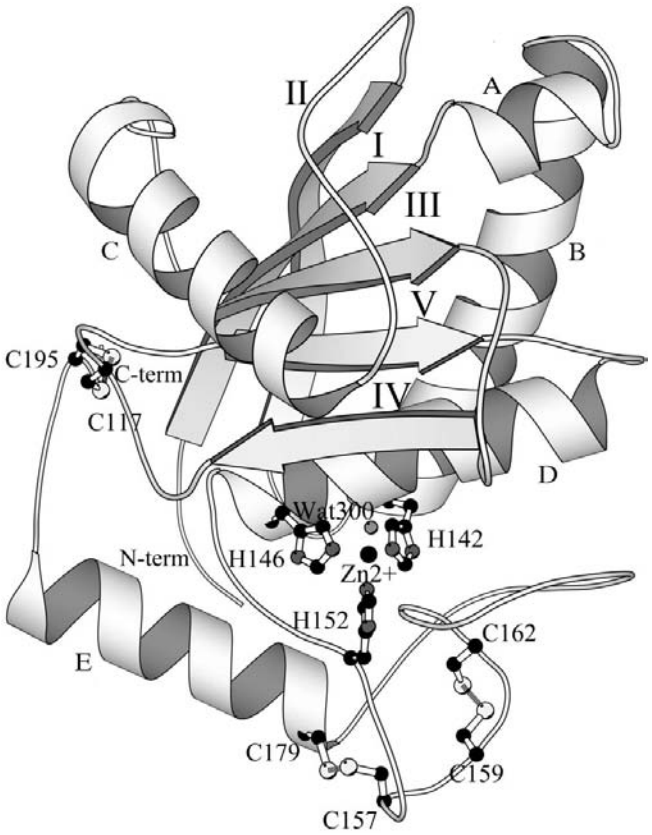

Figure 5
Overall structure of acutolysin-C. The molecule is shown in standard orientation. The three disulfide connections, the zinc ion (filled circle) and the three histidine residues and the catalytic water molecule ligating the zinc ion are also shown. The plot was produced using *MOLSCRIPT* (Kraulis, 1991).

ion and be polarized (Gomis-Rüth *et al.*, 1994). The mechanism of the proteolytic reaction of zinc metalloproteinase(s) may be as follows: the zinc-ligating Water300 is polarized by the carboxylate group of Glu143 and negatively charged, then makes a nucleophilic attack on the positively charged carbonyl C atom of the scissile peptide bond (for the proposed mechanism, see Matthews, 1988; Gomis-Rüth *et al.*, 1994).

Similar to other SVMPs, the proteolytic activity of acutolysin-C depends on the pH value and the optimal activity appears under neutral or weakly alkaline conditions. The structures of acutolysin-A crystallized at different pH values show that the contact distances between the catalytic water molecule and the O atoms of Glu143 carboxylate group in the weakly alkaline structure (with a higher proteolytic activity) are shorter than those in the weakly acidic structure (with a lower proteolytic activity). This small amount of conformational change in the active site is a possible reason why acutolysin-A shows different proteolytic activities at different pH values (Gong *et al.*, 1998). By comparing the available structural data of the P-I class SVMPs, it can be found that the coordination of zinc ion in the active site of all the proteinases is tetrahedral under different pH conditions and that the contact distances between the zinc ion and ligands are not dependent on the crystallization pH values; however, the contact distances between the catalytic water molecule and the O atoms of the Glu143 carboxylate group under neutral or weakly alkaline conditions are shorter than those under weakly acidic conditions (Table 2), and the closer the crystallization pH value is to the optimal activity pH value, the shorter the average distances (Fig. 6). The dependence of the proteolytic activity on pH value may be related to the pK_a of the Glu143 carboxylate group (Gomis-Rüth *et al.*, 1994). The pK_a of a glutamate carboxylate group is about 4.3. Under weakly acidic conditions, the ability of the Glu143 carboxylate group to polarize the catalytic water molecule may be very small and the water molecule may not be sufficiently negatively charged for nucleophilic attack; the proteolytic activity may therefore be low. When the pH value increases to weakly alkaline, the polarization capability of the Glu143 carboxylate group may become stronger and the contact distances between the catalytic water molecule and the Glu143 carboxylate group thus become shorter (Table 2), making the catalytic water molecule fully negatively charged. The distances between Water300 and the Glu143 carboxylate group in the acutolysin-C structure are shorter, which is consistent with the experimental observation that the crystallization pH value is close to its optimal activity pH value.

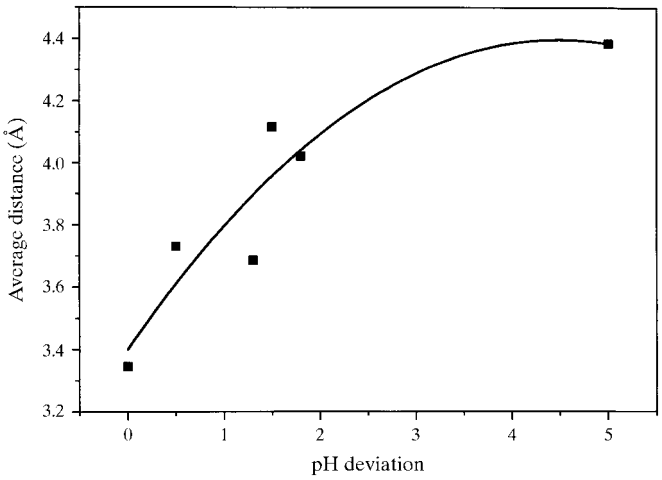

Figure 6
The plot of average distances between the catalytic water molecule and the O atoms of the Glu143 carboxylate group against the pH deviations of the optimal proteolytic activity pH values from the crystallization pH values of P-I class SVMPs.

3.4. Comparison of active-site clefts

Just as in adamalysin II (Gomis-Rüth *et al.*, 1994), in standard orientation the active-site cleft of acutolysin-C is flat from left to right. The left floor of the cleft consists of His191, Ile190, Ser186 and Asn151. The β-sheet segment Val108–Lys114 together with segment His129–Leu135 form the upper edge of the cleft, while segment Pro166–Leu168 separates the S1′ pocket from the solvent area. The S1′ hydrophobic pocket, which contains two water molecules in the acutolysin-C structure, is lined by the side chain of Thr139, the main and side chain of Val108, the main chain of the segment Pro166–Leu168 and the side chain of Leu168. Overall, the active-site clefts of the P-I class SVMPs are similar (Fig. 7). The clefts of acutolysin-A structures at different pH values are almost the same. The cleft of acutolysin-C is more similar to that of H_2-proteinase. Thus, the size of the cleft may not correlate directly with crystallization pH value and the proteolytic activity; the discrepancy of clefts may result from the difference between enzymes. The S1′ pocket of atrolysin C (form d; Botos *et al.*, 1996) has been found to possess a differently shaped entrance and has a 23% larger volume than the corresponding pocket of MMP-8, which suggests

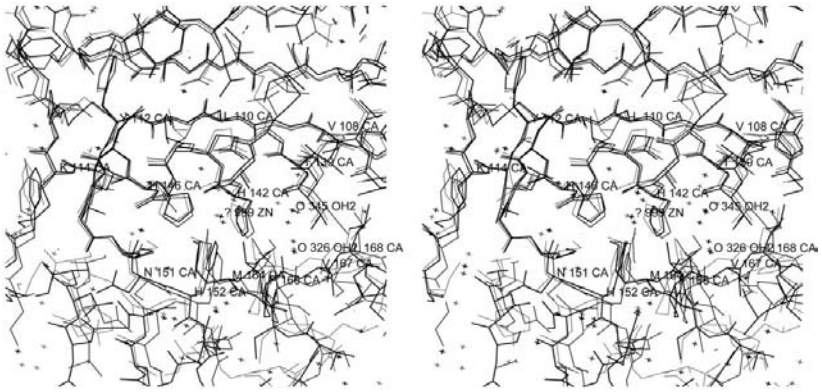

Figure 7
Superposition of the active-site regions and the S1′ pocket of acutolysin-C (thick line), acutolysin-A (moderate line) and adamalysin II (thin line) shown in standard orientation (see Fig. 4). The plot was produced using *CHAIN* (Sack, 1988).

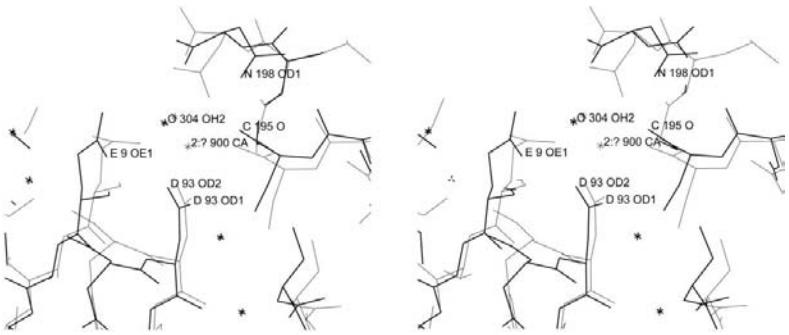

Figure 8
Superposition of calcium ion binding site of acutolysin-A (thin line) and acutolysin-C (thick line). The calcium ion is only included in acutolysin-A. The plot was produced using *CHAIN* (Sack, 1988).

that while atrolysin C (form d) exhibits complete occupancy of the S1′ pocket, it will be unlikely that BB-94 binds human MMP-8 in the same orientation because of the marginally constricted entrance of the pocket. The S1′ hydrophobic pocket of adamalysin II is also larger than that in tumour-necrosis factor-α-converting enzyme (TACE), a member of the matrix metalloproteinase MMP-10 (Cirilli *et al.*, 1997).

3.5. The conformation of the disulfides

The P-I class SVMPs contain two to four disulfide bridges. The sequences published so far have a conserved disulfide bridge, Cys117–Cys195, which connects two subdomains. The number of disulfide bridges varies in the C-terminal subdomain. In addition to the conserved disulfide bridge, acutolysin-C has two further disulfide bridges in this subdomain: Cys157–Cys179 and Cys159–Cys162. Of the SVMP structures, adamalysin II and atrolysin C contain two disulfide bridges and H_2-proteinase and acutolysin-A belong to the three-disulfide enzymes. The conformations of the disulfide bridge Cys117–Cys195 are conserved in all the crystal structures of P-I class SVMP, whereas the conformations and/or number of the disulfide bridges in the C-terminal subdomain are different. The haemorrhagic activities of the snake-venom metalloproteinases are listed in Table 2, which shows that the number of disulfide bridges is not related to the haemorrhagic activity. The proteolytic activities of the metalloproteinases published cannot be compared directly because different methods were utilized for the activity determination. At pH 5.0 and pH 7.5, acutolysin-A shows very similar disulfide-bridge conformation, although it has different proteolytic activities (Gong *et al.*, 1998). Therefore, it seems that the conformations of the disulfide bridges do not play a key role in the proteolytic reaction. This is somewhat paradoxical to the general view about the function of the disulfide bridges.

3.6. The calcium ion binding site

A structural calcium ion occurs on the molecular surface of adamalysin II opposite to the active-site cleft and close to the crossover point of the N-terminal and the C-terminal segments (Gomis-Rüth *et al.*, 1994). This calcium ion is ligated by seven O atoms from Cys197, Asn200, Glu9, Asp93, a water molecule and Gln196 of the adjacent symmetry-related molecule. Of these five residues, Cys197 is strictly conserved and the other four are conserved in most snake-venom metalloproteinases. However, the calcium ion is ligated by seven and six O atoms in weakly acidic and alkaline acutolysin-A structures, respectively (Gong *et al.*, 1998); the common residues are Cys197, Asn200, Glu9, Asp93 and one water molecule; the seventh ligand in alkaline acutolysin-A structure is also a water molecule. No areas representing the calcium ion could be found in the electron-density maps, although these residues are all conserved in acutolysin-C (Fig. 8). The calcium ion may not affect the proteolytic activity as it is far from the active site. Moreover, acutolysin-C and H_2-proteinase have weak and little haemorrhagic activity, respectively, though both proteinases do not have a calcium ion (Table 2). Therefore, it seems that the calcium ion does not directly affect the haemorrhagic activity. Owing to its position close to the C-terminus, the calcium ion could play an important role in the multidomain SVMP structures in stabilizing and tightening the segment connecting the catalytic domain with the succeeding disintegrin-like domain (Gomis-Rüth *et al.*, 1994).

We are indebted to Drs W. Bode, E. F. Meyer and T. Kumasaka for their kind supply of the coordinates of adamalysin II, atrolysin C and H_2-proteinase and to our colleagues in the laboratory for their useful suggestions. This work was supported financially by grants to LN from the Chinese Academy of Science and State Commission of Education of China.

References

Bjarnason, J. B. & Fox, J. W. (1987). *Biochim. Biophys. Acta*, **911**, 356–363.
Bjarnason, J. B. & Fox, J. W. (1994). *Pharmacol. Ther.* **62**, 325–372.
Bjarnason, J. B. & Fox, J. W. (1995). *Methods Enzymol.* **248**, 345–368.
Bjarnason, J. B. & Tu, A. T. (1978). *Biochemistry*, **17**, 3395–3404.
Bode, W., Gomis-Rüth, F. X., Huber, R., Zwilling, R. & Stöcker, W. (1992). *Nature (London)*, **358**, 164–167.
Bode, W., Reinemer, P., Huber, R., Kleine, T., Schnierer, S. & Tschesche, H. (1994). *EMBO J.* **13**, 1263–1269.
Botos, I., Scapozza, L., Zhang, D., Liotta, L. A. & Meyer, E. F. (1996). *Proc. Natl Acad. Sci. USA*, **93**, 2749–2754.
Brünger, A. T. (1992*a*). *X-PLOR, Version 3.1. A System for X-ray Crystallography and NMR.* New Haven: Yale University Press.
Brünger, A. T. (1992*b*). *Nature (London)*, **355**, 472–475.
Chung, M. C. M., Ponnudurai, G., Kataoko, M., Shimizu, S. & Tan, N.-H. (1996). *Arch. Biochem. Biophys.* **325**(2), 199–208.
Cirilli, M., Gallina, C., Gavuzzo, E., Giordano, C., Gomis-Rüth, F. X., Gorini, B., Kress, L. F., Mazza, F., Paradisi, M. P., Pochetti, G. & Politi, V. (1997). *FEBS Lett.* **418**, 319–322.
Collaborative Computational Project, Number 4 (1994). *Acta Cryst.* D**50**, 760–763.
Gomis-Rüth, F. X., Kress, L. F., Kellermann, J., Mayr, I., Lee, X., Huber, R. & Bode, W. (1994). *J. Mol. Biol.* **239**, 513–544.
Gomis-Rüth, F. X., Meyer, E. F., Kress, L. F. & Politi, V. (1998). *Protein Sci.* **7**(2), 283–292.

Gomis-Rüth, F. X., Stöcker, W., Huber, R., Zwilling, R. & Bode, W. (1993). *J. Mol. Biol.* **229**, 945–968.
Gong, W., Teng, M. & Niu, L. (1997). *Sci. China C*, **40**(4), 351–355.
Gong, W., Zhu, X., Liu, S., Teng, M. & Niu, L. (1998). *J. Mol. Biol.* **283**, 657–668.
Gong, W., Zhu, Z., Niu, L. & Teng, M. (1996). *Chin. Sci. Bull.* **41**(6), 544–546.
Hooper, N. M. (1994). *FEBS Lett.* **354**, 1–6.
Jia, L. G., Shimokawa, K. I., Bjarnason, J. B. & Fox, J. W. (1996). *Toxicon*, **34**(11/12), 1269–1276.
Jones, T. A., Zou, J.-Y., Cowan, S. W. & Kjeldgaard, M. (1991). *Acta Cryst.* A**47**, 110–119.
Kraulis, P. J. (1991). *J. Appl. Cryst.* **24**, 946–950.
Kumasaka, T., Yamamoto, M., Moriyama, H., Tanaka, N., Sato, M., Katsube, Y., Yamakawa, Y., Omori-Satoh, T., Iwanaga, S. & Ueki, T. (1996). *J. Biochem.* **119**, 49–57.
Kurecki, T., Laskowski, M. Sr, & Kress, L. F. (1978). *J. Biol. Chem.* **253**(22), 8340–8345.
Laskowski, R. A., MacArthur, M. W., Moss, D. S. & Thornton, J. M. (1993). *J. Appl. Cryst.* **26**, 283–291.
Luzzati, P. V. (1952). *Acta Cryst.* **5**, 802–810.
Matthews, B. W. (1988). *Acc. Chem. Res.* **21**, 333–340.
Minor, W. (1993). *XDISPLAYF Program.* Purdue University, West Lafayette, Indiana, USA.
Navaza, J. (1994). *Acta Cryst.* A**50**, 157–163.
Otwinowski, Z. (1993). *Proceedings of the CCP4 Study Weekend. Data Collection and Processing*, edited by L. Sawyer, N. Isaacs & S. Bailey, pp. 56–62. Warrington: Daresbury Laboratory.
Ownby, C. L. (1990). *Handbook of Toxicology*, edited by W. T. Shier & D. Mebs, pp. 601–654. New York: Marcel Dekker.
Sack, J. S. (1988). *J. Mol. Graph.* **6**, 224–225.
Shannon, J. D., Baramova, E. N., Bjarnason, J. B. & Fox, J. W. (1989). *J. Biol. Chem.* **264**, 11575–11583.
Stöcker, W., Grams, F., Baumann, U., Reinemer, P., Gomis-Rüth, F. X., McKay, D. B. & Bode, W. (1995). *Protein Sci.* **4**, 823–840.
Takeya, H., Arakawa, M., Miyata, T., Iwanaga, S. & Omori-Satoh, T. (1989). *J. Biochem.* **106**, 151–157.
Wolfsberg, T. G., Straight, P. D., Gerena, R. L., Huovila, A.-P. J., Primakoff, P., Myles, D. G. & White, J. M. (1995). *Dev. Biol.* **169**, 378–383.
Xu, X., Wang, C., Liu, J. & Lu, Z. (1981). *Toxicon*, **19**, 633–644.
Zhang, D., Botos, I., Gomis-Rüth, F. X., Doll, R., Blood, C., Njoroge, F. G., Fox, J. W., Bode, W. & Meyer, E. F. (1994). *Proc. Natl Acad. Sci. USA*, **91**, 8447–8451.
Zhu, Z., Gong, W., Zhu, X., Teng, M. & Niu, L. (1997). *Toxicon*, **35**, 283–292.
Zhu, X., Zhu, Z., Gong, W., Teng, M. & Niu, L. (1997). *Acta Biochim. Biophys. Sin.* **29**(2), 163–169.